

3-8-2013

Asymmetry of Magnetosheath Flows and Magnetopause Shape During Low Alfvén Mach Number Solar Wind

B. Lavraud
Universite de Toulouse

E. Larroque
Universite de Toulouse

E. Budnik
Noveltis

V. Génot
Universite de Toulouse

J. E. Borovsky
Space Science Institute

See next page for additional authors

Follow this and additional works at: <https://commons.erau.edu/publication>



Part of the [Astrophysics and Astronomy Commons](#)

Scholarly Commons Citation

Lavraud, B., Larroque, E., Budnik, E., Génot, V., Borovsky, J. E., Dunlop, M. W., Nykyri, K., & et al. (2013). Asymmetry of Magnetosheath Flows and Magnetopause Shape During Low Alfvén Mach Number Solar Wind. *Journal of Geophysical Research: Space Physics*, 118(3). <https://doi.org/10.1002/jgra.50145>

This Article is brought to you for free and open access by Scholarly Commons. It has been accepted for inclusion in Publications by an authorized administrator of Scholarly Commons. For more information, please contact commons@erau.edu.

Authors

B. Lavraud, E. Larroque, E. Budnik, V. Génot, J. E. Borovsky, M. W. Dunlop, K. Nykyri, and et al.

Asymmetry of magnetosheath flows and magnetopause shape during low Alfvén Mach number solar wind

B. Lavraud,^{1,2} E. Larroque,^{1,2} E. Budnik,³ V. Génot,^{1,2} J. E. Borovsky,⁴ M. W. Dunlop,⁵ C. Foullon,⁶ H. Hasegawa,⁷ C. Jacquey,^{1,2} K. Nykyri,⁸ A. Ruffenach,^{1,2} M. G. G. T. Taylor,⁹ I. Dandouras,^{1,2} and H. Rème^{1,2}

Received 23 October 2012; revised 10 January 2013; accepted 18 January 2013; published 8 March 2013.

[1] Previous works have emphasized the significant influence of the solar wind Alfvén Mach number (M_A) on magnetospheric dynamics. Here we report statistical, observational results that pertain to changes in the magnetosheath flow distribution and magnetopause shape as a function of solar wind M_A and interplanetary magnetic field (IMF) clock angle orientation. We use all Cluster 1 data in the magnetosheath during the period 2001–2010, using an appropriate spatial superposition procedure, to produce magnetosheath flow distributions as a function of location in the magnetosheath relative to the IMF and other parameters. The results demonstrate that enhanced flows in the magnetosheath are expected at locations quasi-perpendicular to the IMF direction in the plane perpendicular to the Sun-Earth line; in other words, for the special case of a northward IMF, enhanced flows are observed on the dawn and dusk flanks of the magnetosphere, while much lower flows are observed above the poles. The largest flows are adjacent to the magnetopause. Using appropriate magnetopause crossing lists (for both high and low M_A), we also investigate the changes in magnetopause shape as a function of solar wind M_A and IMF orientation. Comparing observed magnetopause crossings with predicted positions from an axisymmetric semi-empirical model, we statistically show that the magnetopause is generally circular during high M_A , while it is elongated (albeit with moderate statistical significance) along the direction of the IMF during low M_A . These findings are consistent with enhanced magnetic forces that prevail in the magnetosheath during low M_A . The component of the magnetic forces parallel to the magnetopause produces the enhanced flows along and adjacent to the magnetopause, while the component normal to the magnetopause exerts an asymmetric pressure on the magnetopause that deforms it into an elongated shape.

Citation: Lavraud, B., et al. (2013), Asymmetry of magnetosheath flows and magnetopause shape during low Alfvén Mach number solar wind, *J. Geophys. Res. Space Physics*, 118, 1089–1100, doi:10.1002/jgra.50145.

1. Introduction

[2] The response of the Earth’s magnetosphere to the continuous flow of the solar wind is highly variable. Of particular importance are the solar wind velocity and the

direction and strength of the interplanetary magnetic field (IMF). These ingredients combine into the solar wind electric field, a prime parameter affecting the coupling at the dayside magnetosphere through magnetic reconnection, which may lead to geomagnetic storms during strong driving [e.g., *Gonzalez and Mozer*, 1974; *Perreault and Akasofu*, 1978; *Kan and Lee*, 1979]. Another important parameter in solar wind-magnetosphere interaction is the solar wind Alfvén Mach number M_A : the ratio of the bulk solar wind to Alfvén speeds [*Lavraud and Borovsky*, 2008; *Borovsky*, 2008]. This is because M_A directly controls the bow shock compression ratio and the value of the plasma β (ratio of the thermal plasma to magnetic pressures) in the downstream magnetosheath, which in turn changes which of the magnetic or thermal plasma forces dominates the dynamics in the magnetosheath [*Lavraud and Borovsky*, 2008; *Borovsky et al.*, 2009; *Lopez et al.*, 2010, 2011]. As a buffer region between the solar wind and magnetosphere, the magnetosheath plays a pivotal role in the global interaction. When the solar wind M_A is high, thermal plasma forces dominate. When it is low, magnetic forces dominate. This basic

¹Institut de Recherche en Astrophysique et Planétologie, Université de Toulouse (UPS), Toulouse, France.

²Centre National de la Recherche Scientifique, UMR 5277, Toulouse, France.

³Noveltis, 2 Avenue de l’Europe, Ramonville Saint-Agne, France.

⁴Space Science Institute, Boulder, CO, USA.

⁵Rutherford Appleton Laboratory, Chilton, UK.

⁶Centre for Fusion, Space & Astrophysics, University of Warwick, Warwick, UK.

⁷ISAS/JAXA, Sagami-hara, Kanagawa, Japan.

⁸Department of Physical Sciences, Embry-Riddle Aeronautical University, Daytona Beach, FL, USA.

⁹ESTEC/ESA, Noordwijk, The Netherlands.

Corresponding author: B. Lavraud, Institut de Recherche en Astrophysique et Planétologie, Université de Toulouse (UPS), France. (Benoit.Lavraud@irap.omp.eu)

change leads to a dichotomy in the type of solar wind-magnetosphere interaction, in many respects, as synthesized in *Lavraud and Borovsky* [2008] (see also *Vasyliunas* [2004] and *Siscoe* [2011] for complementary discussions to this topic).

[3] Among the various magnetosheath flow properties reported in previous works [e.g., *Howe and Binsack*, 1972; *Petrinec et al.*, 1997; *Paularena et al.*, 2001; *Němeček et al.*, 2000, 2003; *Šafránková et al.*, 2004; *Longmore et al.*, 2005, 2006; *Lavraud et al.*, 2007; *Rosenqvist et al.*, 2007; *Lavraud and Borovsky*, 2008; *Nishino et al.*, 2008; *Erkaev et al.*, 2011, 2012], a particularly drastic change in flows can occur along the magnetopause as first noted by *Chen et al.* [1993]. While in the high M_A case plasma acceleration in the magnetosheath is axisymmetric with respect to the Sun-Earth line (e.g., the hydrodynamic case; *Spreiter et al.* [1966a, 1966b]), for low M_A plasma flow acceleration in the magnetosheath is asymmetric. Owing to the preponderance of asymmetric magnetic forces, with an acceleration directed perpendicular to the magnetic field, plasma flows in the magnetosheath are expected to be significantly lower in the spatial quadrants of the magnetosheath that are aligned with the IMF direction; i.e., above and below the magnetosphere for a north-south oriented IMF. The flows along the flanks for a north-south IMF are, by contrast, much larger and have even been shown to exceed the solar wind speed itself by up to 60% in several cases [*Lavraud et al.*, 2007; *Rosenqvist et al.*, 2007]. Utilizing global magneto-hydrodynamic (MHD) simulations, *Chen et al.* [1993] and *Lavraud et al.* [2007] have shown that it is indeed possible to attain magnetosheath speeds that exceed that of the solar wind thanks to increased magnetic forces in low β plasma. The process is akin to a slingshot-type effect. Despite several case studies noted above, no statistical confirmation and quantification has been performed regarding this process. It is one of the purposes of the present study.

[4] Apart from some debate related to the presence of an indentation at high latitudes near the polar cusps [*Zhou and Russell*, 1997; *Dunlop et al.*, 2000; *Lavraud et al.*, 2002, 2004; *Zhang et al.*, 2007] and dawn-dusk asymmetries [*Dmitriev et al.*, 2004; *Suvorova et al.*, 2005; *Nishino et al.*, 2008], the shape of the magnetopause is often assumed to be axisymmetric about the aberrated Sun-Earth line, i.e., circular. This hypothesis has been used in most empirical models of the magnetopause [e.g., *Sibeck et al.*, 1991; *Petrinec and Russell*, 1996; *Shue et al.*, 1997; *Kawano et al.*, 1999], although models using Artificial Neural Network techniques [*Dmitriev and Suvorova*, 2000] or fits to asymmetric shapes from theoretical expectations [e.g., *Zhuang et al.*, 1981; *Boardsen et al.*, 2000] have also been devised (cf. *Shue and Song* [2002] for a review). *Lavraud and Borovsky* [2008] suggested that, in addition to accelerating flows tailward along the magnetopause, enhanced magnetic forces in the magnetosheath during low M_A exert an asymmetric pressure on the magnetopause so that it may deform and get elongated in the direction of the IMF. This conclusion was based on global MHD simulations alone. It is the second purpose of the present study to test this expectation using spacecraft observations.

[5] In section 2, we present the instrumentation and data used in the study. The methodology and main results are discussed in section 3. Section 4 provides the conclusions.

2. Instrumentation and Model

[6] We primarily use data from the Cluster 1 spacecraft in the 2001–2010 era. The spacecraft flew through the magnetopause and magnetosheath roughly from winter to summer each year. We make use of the ion and magnetic field data from the Cluster Ion Spectrometry (CIS) [*Rème et al.*, 2001] and FluxGate Magnetometer [*Balogh et al.*, 2001] instruments, respectively. The ion data come from the Hot Ion Analyser, which allows measurements of the full 3-D ion distribution functions and moments up to a resolution of 4 s (spin). However, for the statistical analyses, the data are averaged as described in the next sections. Solar wind conditions are mainly taken from the Advanced Composition Explorer (ACE) near L1. A significant part of the data analysis was performed using the functionalities of the AMDA (Automated Multi-Dataset Analysis) web-based tool (<http://cdpp-amda.cesr.fr>).

[7] To further highlight the phenomena of interest here, we performed 3-D global MHD model runs for an event that occurred on 10 November 2002. We used the BATS-R-US model of the solar wind-magnetosphere-ionosphere interaction [*Gombosi et al.*, 2000; *Ridley et al.*, 2004], which is available at the Community Coordinated Modeling Center (<http://ccmc.gsfc.nasa.gov/>). The model is based on the equations of ideal single-fluid MHD. These equations are solved on a three-dimensional grid wherein the cell size increases away from Earth. Further details on the boundary conditions used are given in the next sections.

3. Observations and Discussion

3.1. Magnetosheath Flows and Magnetopause Shape: Case Study

[8] Although case studies of magnetosheath flow acceleration have been reported in past work, these were mainly using stable IMF orientation intervals. To illustrate the asymmetry of magnetosheath flows and the deformation of the magnetopause shape that may occur during low M_A , we first analyze a case when Cluster was suitably located in the magnetosheath during an interval characterized by a low M_A and a slow rotation of the IMF. Figure 1 shows solar wind data for the interval 6:00–19:00 UT on 10 November 2002. Figure 1a shows that this interval was characterized by two distinct periods with high ($M_A > 10$ before 8:20 UT) and low ($M_A < 5$ after 8:20 UT) M_A . The solar wind speed is relatively steady during this interval (Figure 1b; 340–400 km/s). The M_A change comes from a significant drop in density (Figure 1c) and an increase in magnetic field strength (Figure 1e) at the boundary between an interplanetary coronal mass ejection (CME; with low M_A) and its leading sheath (high M_A). The plasma β has a low value (Figure 1d) inside the structure, and the smooth IMF rotation is marked in Figure 1e. These properties make this CME qualify as a magnetic cloud (MC) [*Burlaga et al.*, 1981; *Lepping et al.*, 1990].

[9] Figure 2 shows Cluster 1, ACE, and global MHD simulation results for the Cluster magnetosheath interval 8:45–13:30 UT on 10 November 2002. The global MHD

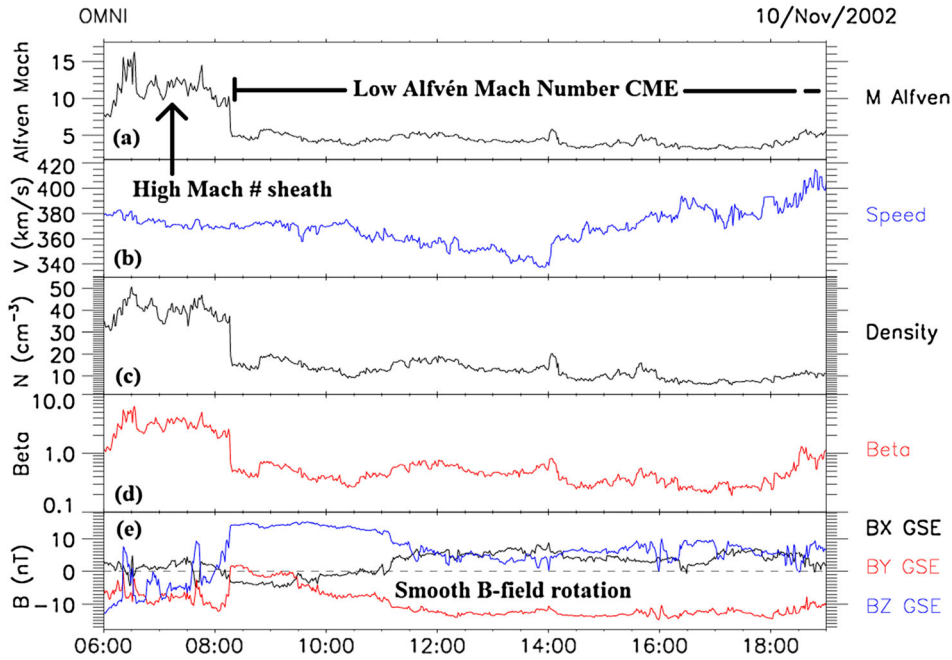


Figure 1. OMNI solar wind data for the interval of interest on 10 November 2002, comprising a low M_A MC with a smooth magnetic field rotation and the high M_A sheath ahead of it. (a) Solar wind M_A , (b) proton bulk speed, (c) proton density, (d) plasma Beta, and (e) magnetic field components in GSE coordinates.

simulation run uses actual ACE solar wind data as input, and the resulting simulated data shown in red are those at the Cluster 1 location. Figures 2a and 2b display the ion energy spectrogram and densities from Cluster during the interval. These data show characteristics typical for the magnetosheath, despite a rather low ion density at Cluster (i.e., not much higher than that measured at ACE), as is expected for low M_A and a lower compression ratio at the bow shock. Focusing on Figure 2c, we note that the lagged solar wind measured by ACE shows a fairly constant speed of ~ 300 – 350 km/s during this interval and that during the first part of the MC the magnetosheath speed at Cluster is almost as large as that in the solar wind itself, on average. Several bursts are observed in the magnetosheath at Cluster with speeds even higher than in the solar wind itself. These may correspond to times of closest approach to the magnetopause, since the speed in the magnetosheath is largest close to the magnetopause (cf. next paragraph), and their intermittent observation may be due to small-scale changes in the distance from the magnetopause to the spacecraft not accounted for in the MHD simulation. The reader is referred to *Lavraud and Borovsky [2008]* for aspects related to enhanced flows and associated magnetopause wave activity during low M_A (see also *Chen et al. [1993]*, *Lavraud et al. [2009]* and *Taylor et al. [2012]*). However, this topic is beyond the focus of the present study.

[10] Figure 3 shows 2-D cuts of the flow speed in the equatorial plane from the global MHD simulation for two times representative of high ($M_A = 9.4$ at 8:00 UT during the MC sheath) and low M_A ($M_A = 3.6$ at 10:30 UT during the MC itself). The shock and magnetopause positions are identified in the figures, with a shock position farther upstream from Earth as expected for lower M_A . What stands

out in those figures is the appearance of strong flows in the magnetosheath (red parts; larger than the solar wind speed itself) adjacent and largest close to the magnetopause during the low M_A MC (Figure 3b), while flows are much smaller during the high M_A sheath (Figure 3a). The fact that the flows are observed on the flanks at 10:30 UT during a primarily northward oriented IMF makes this particular time within the MC very similar to the case studied in *Lavraud et al. [2007]*.

[11] Coming back to Figure 2c, we note a significant drop in the magnetosheath flow speed at Cluster around 11:20 UT, from ~ 350 to ~ 200 km/s. This flow change is concordant with changes in the B_Z (Figure 2d) and B_Y (Figure 2e) components at Cluster in both data and MHD simulation results. It is also consistent with the change in IMF direction observed at ACE within the MC. As can be seen in Figure 2c, a flow decrease is observed in the MHD simulation result at Cluster location, but it is not as large as that actually measured at Cluster.

[12] This change in magnetosheath flow speed is explained by the asymmetry in the dominant magnetic forces in the low β magnetosheath during low M_A . This is illustrated in Figure 4 where GSM Y - Z cuts of the plasma flow at the Cluster location in the simulations are shown during primarily northward (at 10:00 UT; Figure 4a) and north-downward (at 13:00 UT; Figure 4b) IMF clock angle orientations. Figure 4a shows enhanced flows just adjacent to the magnetopause along the flanks, while no such flows are observed above the north and south poles of the magnetosphere (blue regions). This signature is characteristic of the asymmetric magnetic forces that exert forces on the plasma along the flanks but much less over the poles [cf. *Lavraud*

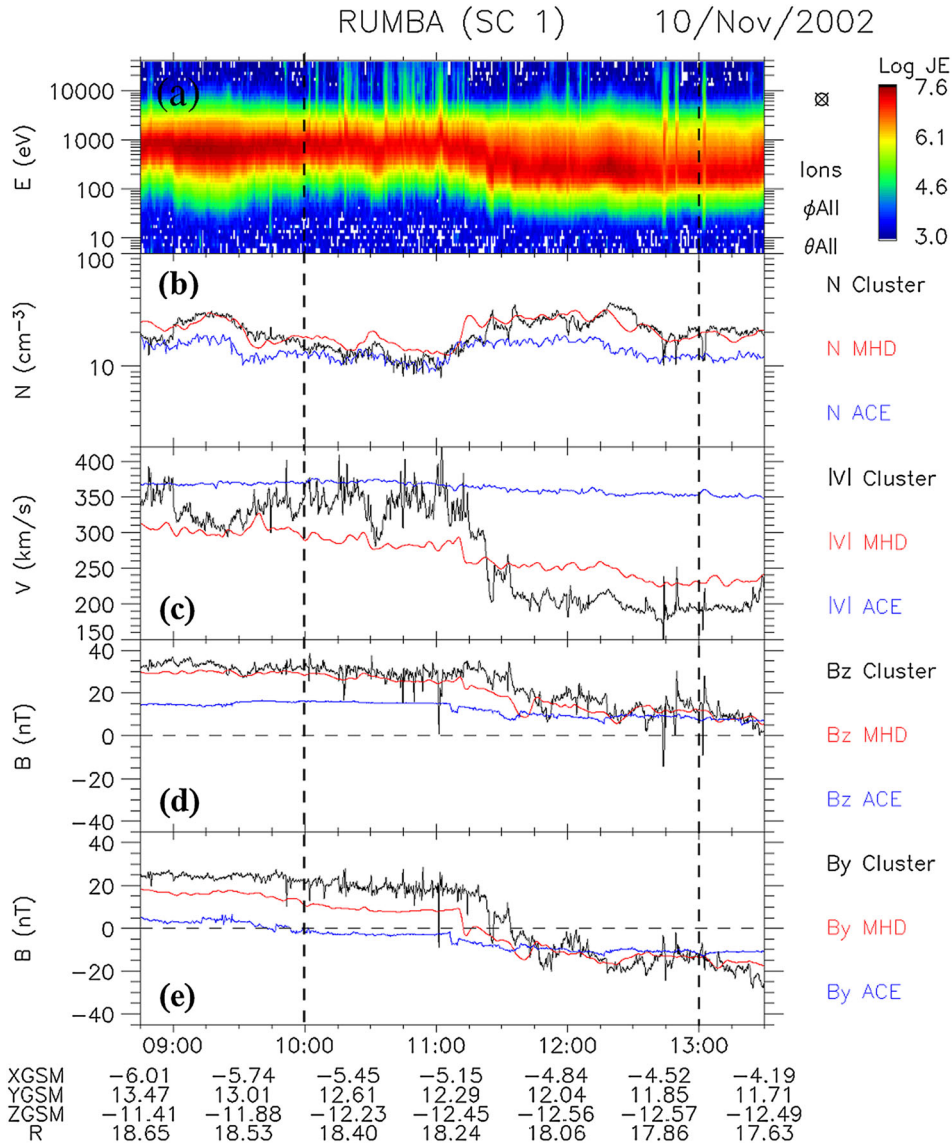


Figure 2. Cluster 1, ACE, and global MHD run data, in GSM coordinates, for the Cluster magnetosheath interval on 10 November 2002. (a) Cluster omnidirectional ion spectrogram. (b) Cluster ion density (black), together with the ACE ion density (blue) and the Global MHD run plasma density (red) at Cluster location. (c) Bulk speeds from Cluster, ACE, and the global MHD run at Cluster location, with same color coding. (d) GSE B_Z and (e) B_Y components of the magnetic field from Cluster, ACE, and the global MHD run at Cluster location, again with the same color coding. ACE solar wind data are lagged by 4000 s to account for advection from ACE to Cluster. The vertical dashed line shows the times used in Figure 4.

et al., 2007]. As the IMF rotates from mainly northward to north-downward during the passage of the MC, the location of the flows changes accordingly, so that Cluster moves out from the enhanced flow region into a slower flow region (Figure 4b). The location of the spacecraft with respect to the enhanced flow region is thus a function of the angle between the IMF orientation and the Earth-centered position vector of the spacecraft, as denoted by θ in Figure 4. As is observed in Figure 4a, Cluster is located slightly outside of the largest flow region, i.e., Cluster is in the greenish region rather than in the narrower red region of enhanced flows just adjacent to the magnetopause. The fact that global MHD results at Cluster location do not reproduce flows as intense

as those actually observed by Cluster in Figure 2c may stem from the magnetopause being somewhat closer to Earth in the simulation than in reality. The grid resolution used for simulations also impacts the magnitude and width of the flow channels, as highlighted by Lavraud and Borovsky [2008]. Another factor is that global ideal MHD simulations cannot produce as intense a plasma depletion layer (PDL) [Zwan and Wolf, 1976] as observed. This may owe to ion kinetic or pressure anisotropy effects being important to generate PDLs, as noted by Meng *et al.* [2012].

[13] In addition to demonstrating the role of IMF orientation in controlling the location of enhanced magnetosheath flows,

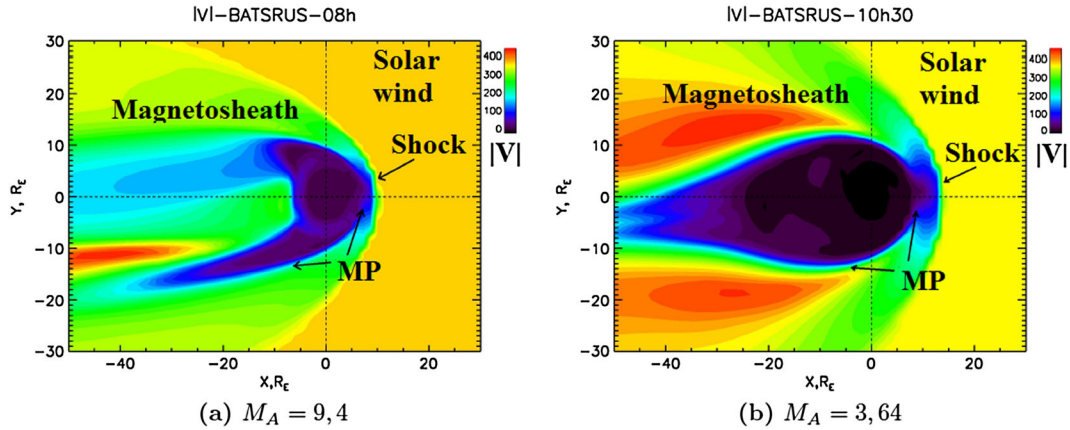


Figure 3. Illustration of the difference in magnetosheath flow distribution for (a) high and (b) low solar wind M_A . In Figure 3a, X - Y plane 2-D cut of the bulk plasma speed (with color palette) from the global MHD simulation at 8:00 UT during the high M_A sheath interval ($M_A = 9.4$). In Figure 3b, Y - Z plane 2-D cut of the bulk plasma speed for the same run but at 10:30 UT during northward IMF in the leading part of the low M_A MC ($M_A = 3.64$). The solar wind flows from the Sun on the right-hand side. The solar wind, bow shock, magnetosheath, and magnetopause (MP) are illustrated.

this case study permits to highlight the influence of magnetic forces on the shape of the magnetopause. Figure 5 shows GSM Y - Z cuts of the current density (used as a proxy for the magnetopause location) from the global MHD simulation respectively at 8:00 UT during the high M_A sheath interval and at 10:30 UT during the low M_A MC interval. This figure is similar to Figure 8 of *Lavraud and Borovsky [2008]* by showing a rather circular magnetopause cross-section for high M_A and a more oblate, elongated shape for low M_A . The elongation occurs along the direction of the IMF and is deemed to result from asymmetric magnetic forces in the low β magnetosheath with enhanced magnetic forces exerted normal to the magnetopause on its flanks. In order to be more quantitative, we show the estimated magnetopause distance as a function of the angle θ —angle away from the northward direction—for both M_A cases in Figure 6. Figure 6 shows the results from an automated search of the peak current density (shown by the dots) in the north-dawn (upper-left) quadrant of the magnetosphere in the simulation. It shows that the magnetopause radius can vary by several R_E as a function of location during low M_A . In section 3.3, we will compare this with a statistical analysis of magnetopause crossings. Note that the angle defined in Figures 5 and 6 is also called θ because it is not fundamentally different from the angle θ defined in Figure 4. The angle in Figures 5 and 6 is indeed the same (clock) angle but for the special case of a virtual spacecraft located at a given magnetopause position and for the special condition of a due northward IMF orientation.

3.2. Statistical Study of Magnetosheath Flows

[14] Together with previous works, the case study of section 3.1 gives strong evidence for the asymmetric flows and associated strong enhancements often seen in the magnetosheath to be the result of the asymmetric magnetic forces that become dominant for low M_A solar wind and low β magnetosheath. This interpretation is further demonstrated here using a statistical approach.

[15] The statistical representation of Figure 7 uses 5 min averages of all available Cluster 1 velocity data during the period 2001–2010. The representation shows the ion speed measured at Cluster normalized to the appropriately lagged ion speed measured at ACE for all available 5 min Cluster data averages ($|V_{\text{SHEATH}}|/|V_{\text{SW}}|$). The statistical data ordering is essentially based on the magnetosheath-interplanetary medium (MIPM) reference frame developed by *Verigin et al. [2006]*. This consists of a spatial superposed analysis which orders spacecraft data from a given time and location relative to models of the magnetopause [*Shue et al., 1997, 1998*] and bow shock positions [*Verigin et al., 2006*]. Using appropriately lagged (using Cluster and ACE spacecraft positions and the measured solar wind velocity at ACE) ACE data as inputs to the models, a fractional position of Cluster in the magnetosheath, relative to the model boundaries (between 0 and 1), is obtained along the direction of the spacecraft position vector (see also *Němčėk et al. [2000, 2003]* for similar procedures). Each data point is then assigned an X and R ($R = \sqrt{Y^2 + Z^2}$) position in the normalized reference frame. The reference solar wind conditions used are a dynamic pressure of 1 nPa and an IMF $B_z = -1$ nT, and data are averaged in $0.5 \times 0.5 R_E$ bins for the distributions shown in Figures 7 to 9. For further details on the method, the reader is referred to *Verigin et al. [2006]* and *Génot et al. [2009, 2011]*. We here use this approach to order normalized magnetosheath flow speeds as a function of the angle between the Cluster position vector and the (lagged) IMF orientation.

[16] Figure 7a shows the statistical results for Cluster data in the magnetosheath during high M_A solar wind (defined here as $M_A > 6$), while Figure 7b shows the results for low M_A solar wind (defined here as $M_A < 5$). The upper and lower parts of Figure 7 show the results for $\theta > 45^\circ$ and $\theta < 45^\circ$, respectively, where θ is defined as the angle between the Cluster position vector and the IMF direction and so that it remains lower than 90° , as depicted in Figure 4. Owing to the limited accuracy of both the bow shock model and the estimated lag time between ACE and Cluster, we

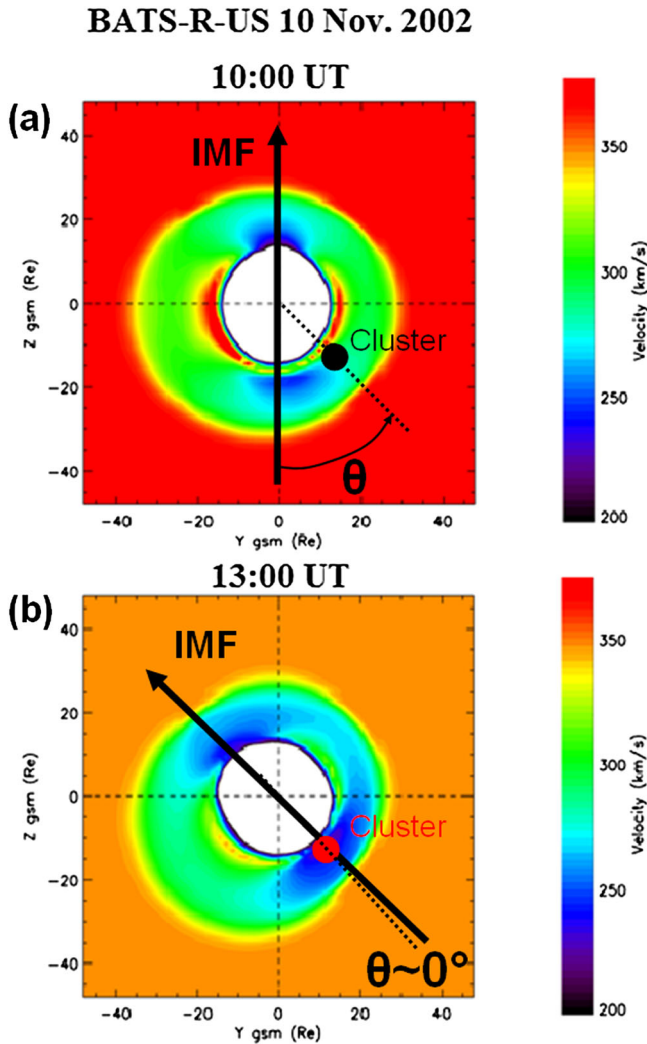


Figure 4. Illustration of the influence of IMF orientation on the location of enhanced flows during low solar wind M_A . Y - Z plane 2-D cuts of the bulk plasma speed (with color palette) are shown from the global MHD simulation during low M_A at (a) 10:00 UT when the IMF was primarily northward, and at (b) 13:00 UT when the IMF had rotated towards dawn by $\sim 45^\circ$. The Y - Z cuts are made at the Cluster location ($X_{\text{GSM}} = -5.6$ and $-4.4 R_E$, respectively), which is shown with a large solid circle. The angle θ used in the statistical analysis of section 3.2 between the direction of the IMF and the Cluster position vector in the Y - Z plane is also illustrated.

implemented a criterion based on the measured flow speed at Cluster. If found to be in the magnetosheath according to the models, Cluster data points that show speeds higher than the lagged solar wind flow speed are removed from analysis since this may mean that measurement was actually made in the solar wind. Although it has been shown that at times the flows in the magnetosheath may be larger than that of the solar wind itself (cf. section 1), such cases are expected to be rare. The use of this condition was thus found (not shown) to smooth the statistical distribution and to remove a number of spurious solar wind data points, while not affecting the statistics nor the basic results of the study.

[17] In Figure 7, all distributions show the expected global acceleration between the subsolar magnetosheath region and locations further downtail. However, for high M_A in Figure 7a, we observe that the flow distributions are similar for $\theta > 45^\circ$ and $\theta < 45^\circ$, while in Figure 7b they are different. The flows for high M_A are overall symmetric, while they are more asymmetric for low M_A . Although much cleaner asymmetries will arise when using local plasma conditions (cf. later discussions), Figure 7b already highlights that larger flows are observed close to the magnetopause at locations past the terminator for low M_A and for $\theta > 45^\circ$, as expected from acceleration through enhanced magnetic forces so that the largest flows are located in quadrants of the magnetosheath quasi-perpendicular to the IMF direction in the GSM Y - Z plane. Note that spurious large speed data points are observed close to the bow shock in Figure 7b. These may be due to solar wind data points that were not removed by our aforementioned condition (e.g., if the ACE-Cluster lag time is not well determined). However, this is not a major issue since our focus is primarily on flows near the magnetopause.

[18] Because the inferred acceleration process is local, in Figure 8 we show results in a similar format for high and low M_A ($M_A > 6$ and $M_A < 5$), but now using a local measurement of the angle between the velocity and magnetic field vectors at Cluster ($\theta_{\text{BV_LOCAL}}$) (instead of the angle between the IMF direction and Cluster position vector). The results are similar to those of Figure 7, although smoother and better structured. These again clearly highlight the strong asymmetric acceleration that occurs during low M_A . Using this local measurement thus permits to remove complexities that arise from draping effects and erroneous advection calculations between ACE and Cluster. Interestingly, even for high M_A in Figure 8a, the flows are larger just adjacent to the magnetopause in the downtail region for $\theta_{\text{BV_LOCAL}} > 45^\circ$ than for $\theta_{\text{BV_LOCAL}} < 45^\circ$ (e.g., small region of low flows (blue/green) in the bottom left corner of the figure). This is consistent with a small asymmetry despite the M_A being high. This highlights the fact that even during (moderately) high M_A , the region of the magnetosheath closest to the magnetopause can have a relatively low plasma β , thus resulting in enhanced magnetic forces, in particular during northward IMF and the formation of a PDL [Farrugia *et al.*, 1995; Phan *et al.*, 1996].

[19] To demonstrate this, Figure 9 shows again a similar representation to Figures 7 and 8 but this time replacing the solar wind M_A thresholds with a condition on the local measurement of the plasma β . Figures 9a and 9b show the statistical results respectively for $\beta > 1$ and $\beta < 1$. This time, Figure 9a is symmetric, illustrating again that under high β conditions the forces that dominantly accelerate the magnetosheath are plasma pressure gradient forces, and those are axisymmetric. Because it is not observed using the local measurement of β , the effect of a PDL as suggested above for Figure 8 is thus confirmed. In Figure 9b, a strong asymmetry is again present with much larger flows for low β and velocity and magnetic field vectors close to perpendicular.

[20] There is not a sufficient amount of Cluster data to build a complete empirical model of magnetosheath flows as a function of M_A (for low values in particular), as is illustrated by the relatively scarce coverage of the magnetosheath in Figure 7b for $M_A < 5$. Adding THEMIS data, although

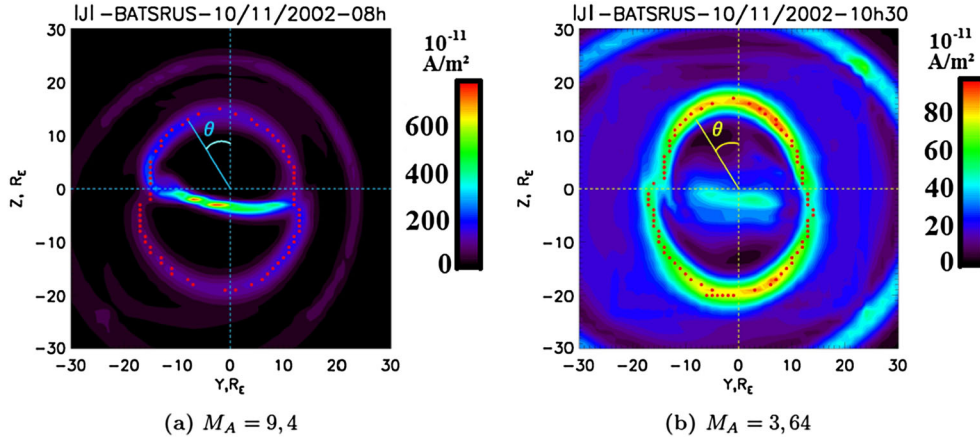


Figure 5. Illustration of the influence of the solar wind M_A on the shape of the magnetopause at $X_{\text{GSM}} = -5 R_E$. Y - Z plane 2-D cuts of the norm of the current density (with color palette) are shown from the global MHD simulation during (a) high M_A ($M_A = 9.4$) and (b) low M_A ($M_A = 3.64$), respectively at 08:00 UT in the high M_A sheath region and at 10:30 UT when the IMF was primarily northward in the low M_A MC. The angle θ displayed is used to illustrate the change in magnetopause location due to the elongation that occurs along the direction of the IMF (primarily northward in Figure 5b) during low M_A . The dots represent the peak in current density found using an automated scheme and meant to represent the magnetopause location.

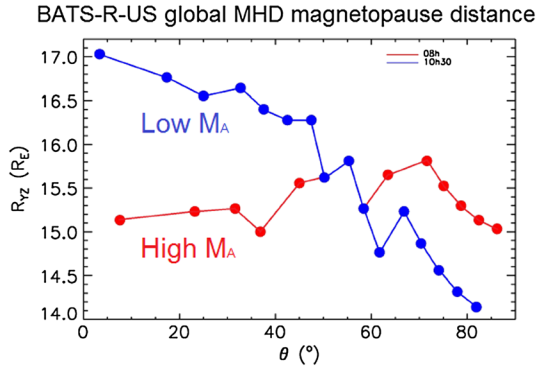


Figure 6. Dependence of the magnetopause position, as defined by the peak current density (dots), on the angle θ from the north direction in the Y - Z plane in Figure 5. The red and blue curves are for the magnetopause position in the north-down quadrant for high ($M_A = 9.4$) and low ($M_A = 3.64$) M_A solar wind conditions, respectively.

desirable in the future, would not help in obtaining much more low M_A occurrences since the mission has primarily been operating during solar cycle minimum when M_A is typically high (e.g., less MCs). This statistical study yet provides a definite proof of the significant influence of the solar wind M_A , and in turn of the magnetosheath plasma β , on magnetosheath flows.

3.3. Statistical Study of the Magnetopause Shape

[21] In this section, we show the results of an analysis meant to test the expected elongated magnetopause shape during low M_A solar wind. For that purpose, we use two magnetopause crossing lists. The first list of magnetopause crossings was taken from that compiled in the context of a

study by *Wang et al.* [2006] for the period 2001–2003. We here only use the 297 crossings from that list for which the lagged ACE data showed $M_A > 6$. To build the second magnetopause crossing list, using AMDA we automatically searched for low solar wind M_A periods (defined as $M_A < 5$) during 2001–2006 and visually identified a total of 241 magnetopause crossings by Cluster 1. The time, location, and lagged solar wind conditions that prevailed during all those crossings were recorded (based on a 10 min average each side of the crossing time).

[22] As illustrated in Figure 5b for a time when the IMF is directed northward, the magnetopause distance from Earth may be expected to be largest for small values of the angle θ and smallest for values close to 90° . Again, in Figure 5b, θ is the angle in the GSM Y - Z plane between the north (which is also essentially the direction of the IMF) and the position vector of the part of the magnetopause being considered. It is defined in the range $[0, 90^\circ]$. Since the IMF orientation is variable, the expected direction of elongation of the magnetopause shape during low M_A should vary as well. The elongation is expected to follow the direction of the IMF. Therefore, in order to increase the statistics (i.e., rather than limiting ourselves to only pure north-south IMF orientations), we here consider the distance of all magnetopause crossings from our lists as a function of the angle between the IMF orientation and the position vector of the spacecraft at the time of the crossing. This clock angle θ is the same as that represented in Figure 5 but in the more general case of a variable IMF clock angle direction, as depicted in Figure 4.

[23] In order to highlight a relative change in magnetopause shape, the observed magnetopause distances from our crossings lists are then compared to the *Shue et al.* [1997, 1998] model for the prevailing solar wind conditions (with IMF B_Z and dynamic pressure as input). We here use the difference ($R_{\text{REAL}} - R_{\text{SHUE}}$) between the observed and

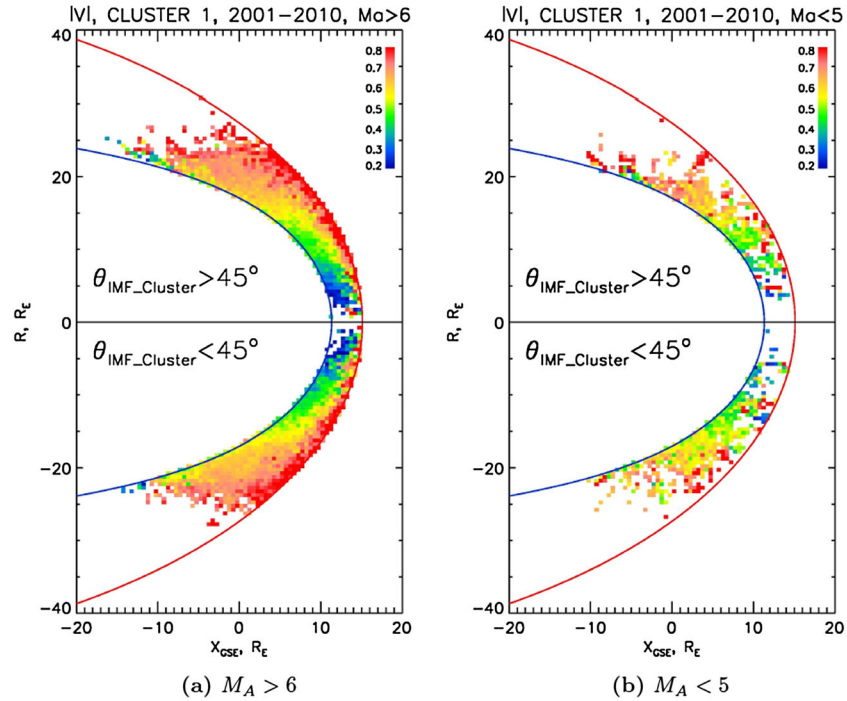


Figure 7. Statistical distribution of the magnetosheath ion speed measured at Cluster normalized to the appropriately lagged ion speed measured at ACE for each 5 min data averages; a color palette of $|V_{\text{SHEATH}}|/|V_{\text{SW}}|$ is given in the top right corner. The statistical data ordering is based on the magnetosheath-interplanetary medium (MIPM) reference frame developed by *Verigin et al.* [2006], using models of the magnetopause [*Shue et al.*, 1997, 1998] and bow shock positions [*Verigin et al.*, 2006] with appropriately lagged ACE data as inputs. Each data point is assigned an X and R ($R = \sqrt{Y^2 + Z^2}$) position in the normalized reference frame. The reference solar wind conditions used are a dynamic pressure of 1 nPa and an IMF $B_Z = -1$ nT, and data are averaged in $0.5 \times 0.5 R_E$ bins. (a) Distributions for high $M_A > 6$. (b) Distributions for low $M_A < 5$. In each M_A case, the top panel shows the results for an angle θ between the IMF direction and the Cluster position vector in the GSM Y - Z plane $> 45^\circ$, i.e., quasi-perpendicular to the IMF. The bottom panels show results for $\theta < 45^\circ$, i.e., quasi-parallel. See text for further details.

modeled magnetopause distances. The logic of this normalization comes from the fact that this magnetopause model is axisymmetric relative to the Sun-Earth line, and thus any elongation should be readily seen by contrasting the observed magnetopause distance with the model expectation.

[24] Figure 10 shows selected outputs of our analysis as explained above. It shows scatter plots of the difference between the observed and modeled magnetopause distances as a function of the angle θ between the IMF orientation and the spacecraft position in the GSM Y - Z plane at the time of magnetopause crossing. Figure 10a shows the results for crossings from the list of *Wang et al.* [2006] which have solar wind $M_A > 6$. Figure 10b shows the results for the list we compiled based on the selection of $M_A < 5$ over the period 2001–2006. In Figure 10a, we show three correlation analyses to the scatter plot for three ranges of magnetopause downtail distances ($X_{\text{GSE}} < 0 R_E$; $0 R_E < X_{\text{GSE}} < 15 R_E$; $5 R_E < X_{\text{GSE}} < 15 R_E$). All fits show a negligible slope as a function of the angle θ (see also Table 1). This is consistent with the magnetopause being generally circular for high M_A solar wind conditions. It should be noted that the dayside crossings (pink and purple curves) are overall

consistent with the model ($R_{\text{REAL}} - R_{\text{SHUE}} \sim 0 R_E$), while results for the more downtail crossings (red curve) suggest that actual magnetopause crossings are on average farther from Earth than estimated by the model. This may be explained by a lack of sufficient downtail magnetopause crossings in the parameterization of the Shue et al. model, with a larger tail flaring [e.g., *Sibeck et al.*, 1986].

[25] By contrast, Figure 10b shows the scatter plot and correlation analysis to the data for the case of low $M_A (< 5)$ magnetopause crossings in the range $-10 R_E < X_{\text{GSE}} < 10 R_E$. In spite of a moderate correlation coefficient (c.c. = -0.47), the results show that observed magnetopause crossings are typically closer to Earth when the position vector of the magnetopause crossing is quasi-perpendicular to the IMF in the GSM Y - Z plane, while farther if it is quasi-parallel. This is in accord with an elongated magnetopause shape during low M_A that follows the IMF orientation. Table 2 shows the result of correlation analyses to various subsets of the low M_A crossings as a function of the threshold M_A used (4 or 5), as well as a function of a range of X_{GSE} crossing locations. The analyses on all these subsets of crossings confirm the aforementioned trend, with similar and negative

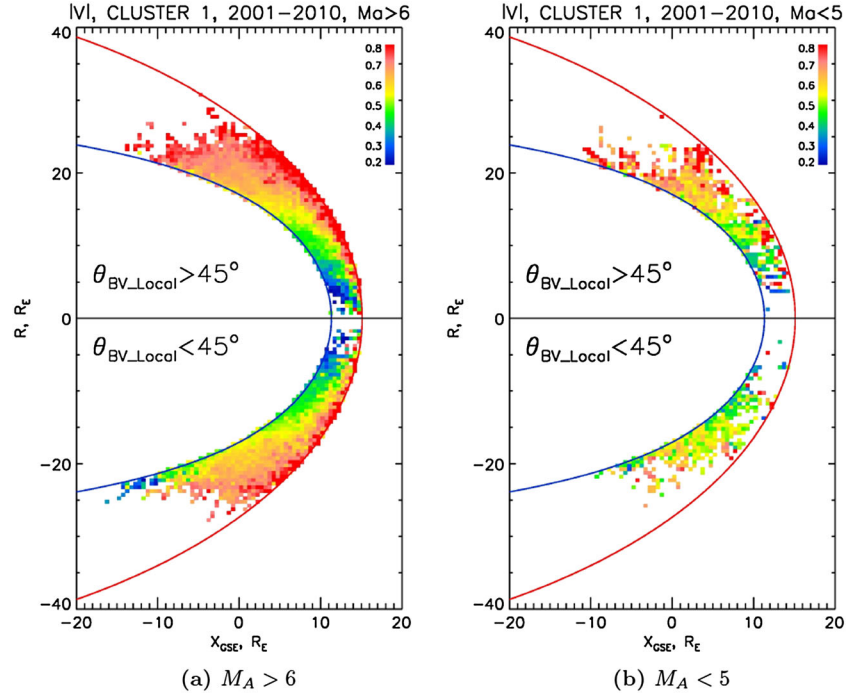


Figure 8. Same as Figure 7, but this time in each M_A case, the top panel shows the results as a function of the angle θ_{BV_Local} between the ion velocity and magnetic field directions locally measured at Cluster for the case of quasi-perpendicular ($\theta_{BV_Local} > 45^\circ$) magnetic field and flow. The bottom distributions show the case of quasi-parallel magnetic field and flow ($\theta_{BV_Local} < 45^\circ$). See text for further details.

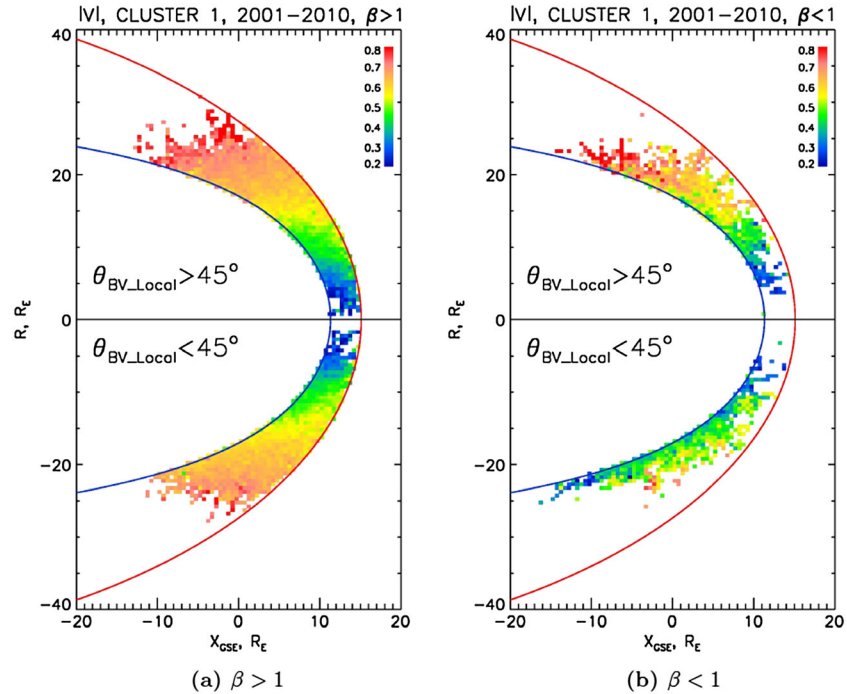


Figure 9. Same as Figure 8, but this time the panels show the distributions of the normalized magnetosheath flow as a function of the plasma β (and θ_{BV_Local} as in Figure 8) locally measured at Cluster, respectively for values larger and lower than 1. See text for further details.

correlation coefficients (between -0.417 and -0.493), consistent with an elongation of the magnetopause along the IMF direction. Only the small subset using crossings at far downtail

locations is incompatible, but this is most likely due to the small statistics in this particular position range and the higher variability of the magnetopause location at larger downtail distances.

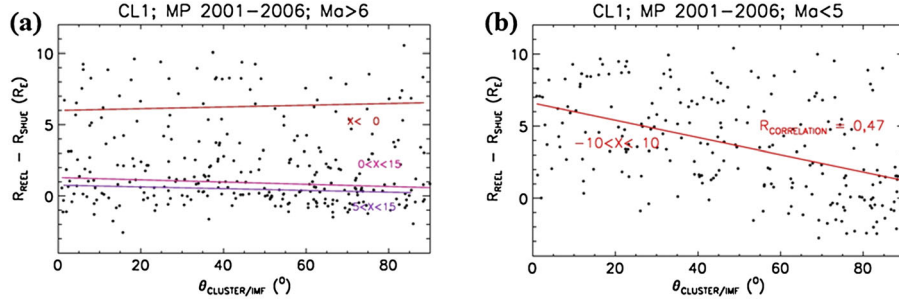


Figure 10. Scatter plots of the difference between the observed and modeled magnetopause distances as a function of the angle θ between the IMF orientation and the spacecraft position in the GSM Y - Z plane at the time of crossing for (a) high $M_A > 6$ and (b) low $M_A < 5$ magnetopause lists (as detailed in text). Correlation coefficients are shown for three subsets of magnetopause crossing downtail distances in Figure 10a, while only one subset and its correlation coefficient are given in Figure 10b. Other magnetopause subsets have been analyzed and are reported in Tables 1 and 2. See text for discussion.

Table 1. Results of the Correlation Analysis of Relative Magnetopause Distances^a as a Function of the Angle θ between the IMF Direction and Magnetopause Crossing Location in the GSM Y - Z Plane, in the Case of High $M_A > 6$ and for Three Magnetopause Downtail Location Ranges^b

M_A Threshold	X_{GSE} Range	Correlation Coefficient	Number of Points
$M_A > 6$	$X_{GSE} < 0$	0.0629	67
	$0 < X_{GSE} < 15$	-0.121	220
	$5 < X_{GSE} < 15$	-0.138	91

^aObserved distance normalized to model distance: $R_{REAL} - R_{SHUE}$.

^bThe respective number of magnetopause crossings is also indicated.

Table 2. Results of the Correlation Analysis of Relative Magnetopause Distances^a as a Function of the Angle θ Between the IMF Direction and Magnetopause Crossing Location in the GSM Y - Z Plane, in the Case of Low M_A (Both $M_A < 4$ and $M_A < 5$) and for Seven Subsets of Magnetopause Downtail Location Ranges^b

M_A Threshold	X_{GSE} Range	Correlation Coefficient	Number of Points
$M_A < 4$	$X_{GSE} < -10$	0.836	15
	$-10 < X_{GSE} < 15$	-0.421	111
	$-5 < X_{GSE} < 15$	-0.427	101
	$0 < X_{GSE} < 15$	-0.417	71
	$5 < X_{GSE} < 15$	-0.474	38
	$-10 < X_{GSE} < 10$	-0.447	109
	$-5 < X_{GSE} < 10$	-0.456	99
$M_A < 5$	$X_{GSE} < -10$	0.839	16
	$-10 < X_{GSE} < 15$	-0.456	225
	$-5 < X_{GSE} < 15$	-0.466	202
	$0 < X_{GSE} < 15$	-0.470	143
	$5 < X_{GSE} < 15$	-0.426	62
	$-10 < X_{GSE} < 10$	-0.469	223
	$-5 < X_{GSE} < 10$	-0.481	200
	$0 < X_{GSE} < 10$	-0.493	141
	$5 < X_{GSE} < 10$	-0.471	60

^aObserved distance normalized to model distance: $R_{REAL} - R_{SHUE}$.

^bThe respective number of magnetopause crossings is also indicated.

4. Conclusions

[26] The present study was meant to address several purposes: (1) provide quantitative spatial distributions of magnetosheath flows as a function of solar wind M_A , IMF

clock angle orientation, and other local parameters, (2) statistically confirm the occurrence of enhanced flows adjacent to the magnetopause during low M_A (and function of IMF orientation), and (3) provide a direct test of a possible asymmetry in magnetopause shape during low M_A .

[27] The main results are as follows:

[28] 1. The statistical, spatial superposed analysis demonstrates that magnetosheath flow distributions are axisymmetric about the Sun-Earth line during high M_A . This is compatible with the magnetosheath flow acceleration being dominated by thermal plasma pressure forces, which are not ordered by the magnetic field orientation.

[29] 2. The analysis confirms that during low M_A and subsequent low magnetosheath β , magnetic forces become preponderant and act to accelerate magnetosheath flows preferentially in spatial quadrants quasi-perpendicular to the IMF direction in the GSM Y - Z plane. This stems from the anisotropy of magnetic forces, so that the largest acceleration occurs at locations in the magnetosheath where the flows and magnetic field are orthogonal.

[30] 3. These latter assertions are confirmed from the statistical analysis using conditions on local measurements in the magnetosheath, namely, the plasma β and the angle between the plasma velocity and magnetic field. Our findings also confirm that the influence of magnetic forces increases close to the magnetopause where the plasma and magnetic field further pile up and drape over the magnetopause, such as through the formation of a PDL.

[31] 4. The possibility of magnetopause shape elongation along the IMF direction during low M_A , as proposed by *Lavraud and Borovsky* [2008] based on global MHD simulations, is demonstrated based on the comparison of magnetopause positions for low and high M_A with those expected from an axisymmetric magnetopause model. This elongation is the result of the aforementioned enhanced magnetic forces—the tangential component of which leads to the enhanced flows along the magnetopause—which also exert a force normal to the magnetopause.

[32] 5. The elongation is shown to follow changes in IMF orientation. Differences in magnetopause radial distances is shown to be of order $5 R_E$ (on average for the given conditions of Figure 10) when comparing magnetopause distances at locations quasi-parallel and quasi-perpendicular to the IMF orientation for the given magnetopause dataset (for times

when $M_A < 5$). How large this elongation may be during extreme cases remains unknown.

[33] 6. These results, and in particular those pertaining to dynamical changes in flows and magnetopause shape as a function of IMF orientation (not addressed much in previous works), are consistent with the results from a global MHD simulation run for a pertinent case study during the passage of a low M_A MC with a preceding, higher M_A sheath region.

[34] In view of the limited statistics for $M_A < 5$ in the spatial superposed distributions, the building of a detailed and quantitative empirical model of magnetosheath properties that specifically accounts for low M_A solar wind conditions will require the inclusion of much more data from all past and upcoming magnetospheric missions. Much further work is required to develop a full understanding of magnetosheath physics and of how magnetosheath properties affect solar wind-magnetosphere interaction in many important ways [e.g., Lavraud and Borovsky, 2008; Lopez et al., 2010, 2011].

[35] **Acknowledgments.** The authors thank all Cluster instrument teams for their efforts in the development of the instruments and in the generation of the datasets. This work was performed in part thanks to the dynamics of ISSI working groups and of the NSF/GEM program. The statistical analyses performed used tools developed by the CDPP (Centre de Données de la Physique des Plasmas—<http://cdpp.cesr.fr>) at IRAP (Institut de Recherche en Astrophysique et Planétologie, Toulouse), such as the AMDA web-based tool (Automated Multi-Dataset Analysis: <http://cdpp-amda.cesr.fr>). We thank the ACE MFI and SWEPAM instruments teams, the CDAWeb, and the OMNI teams for providing solar wind data. We also thank the Community Coordinated Modeling Center (CCMC; <http://ccmc.gsfc.nasa.gov/>) for the use of BATS-R-US global MHD runs. M.W.D. acknowledges support from the Chinese Academy of Sciences (CAS) visiting Professorship program for senior international scientists, grant no. 2012T1G0018.

References

- Balogh, A., et al. (2001), The Cluster magnetic field investigation: Over-view of in-flight performance and initial results, *Ann. Geophys.*, *19*(10–12), 1207–1217.
- Boardsen, S. A., T. E. Eastman, T. Sotirelis, and J. L. Green (2000), An empirical model of the high-latitude magnetopause, *J. Geophys. Res.*, *105*, 23193.
- Borovsky, J. E. (2008), The rudiments of a theory of solar wind/magnetosphere coupling derived from first principles, *J. Geophys. Res.*, *113*, A08228, doi:10.1029/2007JA012646.
- Borovsky, J. E., B. Lavraud, and M. M. Kuznetsova (2009), Polar-cap saturation, dayside reconnection and changes to the magnetosphere, *J. Geophys. Res.*, *114*, A03224, doi:10.1029/2009JA014058.
- Burlaga, L. F., E. Sittler, F. Mariani, and R. Schwenn (1981), Magnetic loop behind an interplanetary shock: Voyager, Helios, and IMP 8 observations, *J. Geophys. Res.*, *86*(A8), 6673–6684, doi:10.1029/JA086iA08p06673.
- Chen, S.-H., M. G. Kivelson, J. T. Gosling, R. J. Walker, and A. J. Lazarus (1993), Anomalous aspects of magnetosheath flow and of the shape and oscillations of the magnetopause during an interval of strongly northward interplanetary magnetic field, *J. Geophys. Res.*, *98*(A4), 5727–5742.
- Dmitriev, A. V., and A. V. Suvorova (2000), Three-dimensional artificial neural network model of the dayside magnetopause, *J. Geophys. Res.*, *105*, 18909.
- Dmitriev, A. V., A. V. Suvorova, J. K. Chao, and Y.-H. Yang (2004), Dawn-dusk asymmetry of geosynchronous magnetopause crossings, *J. Geophys. Res.*, *109*, A05203, doi:10.1029/2003JA010171.
- Dunlop, M. W., P. J. Cargill, T. J. Stubbs, and P. Wooliams (2000), The high-altitude cusps: HEOS-2, *J. Geophys. Res.*, *105*(A12), 27,509–27,517.
- Erkaev, N. V., C. J. Farrugia, B. Harris, and H. K. Biernat (2011), On accelerated magnetosheath flows under northward IMF, *Geophys. Res. Lett.*, *38*, L01104, doi:10.1029/2010GL045998.
- Erkaev, N. V., C. J. Farrugia, A. V. Mezentssev, R. B. Torbert, and H. K. Biernat (2012), Accelerated magnetosheath flows caused by IMF draping: Dependence on latitude, *Geophys. Res. Lett.*, *39*, L01103, doi:10.1029/2011GL050209.
- Farrugia, C. J., N. V. Erkaev, H. K. Biernat, and L. F. Burlaga (1995), Anomalous magnetosheath properties during Earth passage of an interplanetary magnetic cloud, *J. Geophys. Res.*, *100*(A10), 19,245–19,257.
- Génot, V., E. Budnik, P. Hellinger, T. Passot, G. Belmont, P. M. Travnicek, P. L. Sulem, E. Lucek, and I. Dandouras (2009), Mirror structures above and below the linear instability threshold: Cluster observations, fluid model and hybrid simulations, *Ann. Geophys.*, *27*(2), 601–615.
- Génot, V., L. Broussillou, E. Budnik, P. Hellinger, P. M. Travnicek, E. Lucek, and I. Dandouras (2011), Timing mirror structures observed by Cluster with a magnetosheath flow model, *Ann. Geophys.*, *29*(10), 1849–1860, doi:10.5194/angeo-29-1849-2011.
- Gombosi, T. I., et al. (2000), Multiscale MHD simulation of a coronal mass ejection and its interaction with the magnetosphere-ionosphere system, *J. Atmos. Sol. Terr. Phys.*, *62*(16), 1515–1525.
- Gonzalez, W. D., and F. S. Mozer (1974), A quantitative model for the potential resulting from reconnection with an arbitrary interplanetary magnetic field, *J. Geophys. Res.*, *79*(28), 4186–4194.
- Howe, H. C., and J. H. Binsack (1972), Explorer 33 and 35 plasma observations of magnetosheath flow, *J. Geophys. Res.*, *77*(19), 3334–3344.
- Kan, J. R., and L. C. Lee (1979), Energy coupling function and solar wind-magnetosphere dynamo, *Geophys. Res. Lett.*, *6*(7), 577–580.
- Kawano, H., S. M. Petrinc, C. T. Russell, and T. Higuchi (1999), Magnetopause shape determinations from measured position and estimated flaring angle, *J. Geophys. Res.*, *104*(A1), 247–261.
- Lavraud, B., et al. (2002), Cluster observations of the exterior cusp and its surrounding boundaries under northward IMF, *Geophys. Res. Lett.*, *29*(20), 56.
- Lavraud, B., A. Fedorov, E. Budnik, A. Grigoriev, P. J. Cargill, M. W. Dunlop, H. Réme, I. Dandouras, and A. Balogh (2004), Cluster survey of the high-altitude cusp properties: A three-year statistical study, *Ann. Geophys.*, *22*(8), 3009–3019.
- Lavraud, B., J. E. Borovsky, A. J. Ridley, E. W. Pogue, M. F. Thomsen, H. Réme, A. N. Fazakerley, and E. A. Lucek (2007), Strong bulk plasma acceleration in Earth's magnetosheath: A magnetic slingshot effect?, *Geophys. Res. Lett.*, *34*, L14102, doi:10.1029/2007GL030024.
- Lavraud, B., and J. E. Borovsky (2008), Altered solar wind-magnetosphere interaction at low Mach numbers: Coronal mass ejections, *J. Geophys. Res.*, *113*, A00B08, doi:10.1029/2008JA013192.
- Lavraud, B., et al. (2009), Tracing solar wind plasma entry into the magnetosphere using ion-to-electron temperature ratio, *Geophys. Res. Lett.*, *36*, L18109, doi:10.1029/2009GL039442.
- Lepping, R. P., J. A. Jones, L. F. Burlaga (1990), Magnetic field structure of interplanetary magnetic clouds at 1 AU, *J. Geophys. Res.*, *95*(A8), 11,957–11,965, doi:10.1029/JA095iA08p11957.
- Longmore, M., S. J. Schwartz, J. Geach, B. M. A. Cooling, I. Dandouras, E. A. Lucek, and A. N. Fazakerley (2005), Dawn-dusk asymmetries and sub-Alfvénic flow in the high and low latitude magnetosheath, *Ann. Geophys.*, *23*, 3351–3364.
- Longmore, M., S. J. Schwartz, and E. A. Lucek (2006), Rotation of the magnetic field in Earth's magnetosheath by bulk magnetosheath plasma flow, *Ann. Geophys.*, *24*, 339–354.
- Lopez, R. E., R. Bruntz, E. J. Mitchell, M. Wiltberger, J. G. Lyon and V. G. Merkin (2010), Role of magnetosheath force balance in regulating the dayside reconnection potential, *J. Geophys. Res.*, *115*, A12216, doi:10.1029/2009JA014597.
- Lopez, R. E., V. G. Merkin, and J. G. Lyon (2011), The role of the bow shock in solar wind-magnetosphere coupling, *Ann. Geophys.*, *29*(6), 1129–1135.
- Meng, X., G. Tóth, M. W. Liemohn, T. I. Gombosi, and A. Runov (2012), Pressure anisotropy in global magnetospheric simulations: A magnetohydrodynamics model, *J. Geophys. Res.*, *117*, A08216, doi:10.1029/2012JA017791.
- Němeček, Z., J. Šafránková, G. N. Zastenker, P. Pisoft, K. I. Paularena, and J. D. Richardson (2000), Observations of the radial magnetosheath profile and a comparison with gasdynamic model predictions, *Geophys. Res. Lett.*, *27*(17), 2801–2804.
- Němeček, Z., M. Hayosh, J. Šafránková, G. N. Zastenker, and J. D. Richardson (2003), The dawn-dusk asymmetry of the magnetosheath: INTERBALL observations, *Adv. Space Res.*, *31*(5), 1333–1340.
- Nishino, M. N., M. Fujimoto, T.-D. Phan, T. Mukai, Y. Saito, M. M. Kuznetsova, and L. Rastätter (2008), Anomalous flow deflection at Earth's low-Alfvén-Mach-number bow shock, *Phys. Rev. Lett.*, *101*, 065003.
- Paularena, K. I., J. D. Richardson, M. A. Kolpak, C. R. Jackson, and G. Siscoe (2001), A dawn-dusk density asymmetry in Earth's magnetosheath, *J. Geophys. Res.*, *25*, 377–25 394, doi:10.1029/2000JA000177.
- Perreault, P., and S.-I. Akasofu (1978), A study of geomagnetic storms, *Geophys. J. R. Astron. Soc.*, *54*, 547–573.
- Petrinc, S. M., and C. T. Russell (1996), Near-Earth magnetotail shape and size as determined from the magnetopause flaring angle, *J. Geophys. Res.*, *101*(A1), 137–152.

- Petrinec, S. M., T. Mukai, A. Nishida, T. Yamamoto, T. K. Nakamura, and S. Kokubun (1997), Geotail observations of magnetosheath flow near the magnetopause, using Wind as a solar wind monitor, *J. Geophys. Res.*, *102*(A12), 26,943–26,959.
- Phan, T.-D., and G. Paschmann (1996), Low-latitude dayside magnetopause and boundary layer for high magnetic shear. 1. Structure and motion, *J. Geophys. Res.*, *101*(A4), 7801–7815, doi:10.1029/95JA03752.
- Phan, T.-D., G. Paschmann, W. Baumjohann, N. Sckopke, and H. Lühr (1994), The magnetosheath region adjacent to the dayside magnetopause: AMPTE/IRM observations, *J. Geophys. Res.*, *99*(A1), 121–141, doi:10.1029/93JA02444.
- Rème, H., et al. (2001), First multispacecraft ion measurements in and near the Earth's magnetosphere with the identical CLUSTER Ion Spectrometry (CIS) Experiment, *Ann. Geophys.*, *19*(10–12), 1303–1354.
- Ridley, A. J., T. I. Gombosi, and D. L. DeZeeuw (2004), Ionospheric control of the magnetosphere: Conductance, *Ann. Geophys.*, *22*(2), 567–584.
- Rosenqvist, L., A. Kullen, and S. Buchert (2007), An unusual giant spiral arc in the polar cap region during the northward phase of a coronal mass ejection, *Ann. Geophys.*, *25*, 507–517.
- Šafránková, J., M. Hayosh, Z. Němeček, and L. Prech (2004), Magnetosheath investigations: Interball contribution to the topic, in *Multiscale Processes in the Earth's Magnetosphere: From Interball to Cluster*, pp. 73–94, Kluwer Academic Publishers, Dordrecht, The Netherlands.
- Shue, J.-H., J. K. Chao, H. C. Fu, C. T. Russell, P. Song, K. K. Khurana, and H. J. Singer (1997), A new functional form to study the solar wind control of the magnetopause size and shape, *J. Geophys. Res.*, *102*(A5), 9497–9511.
- Shue, J.-H., et al. (1998), Magnetopause location under extreme solar wind conditions, *J. Geophys. Res.*, *103*(A8), 17691–17700.
- Shue, J.-H., and P. Song (2002), The location and shape of the magnetopause, *Planet. Space Sci.*, *50*(5–6), 549–558.
- Sibeck, D. G., G. L. Siscoe, J. A. Slavin, and R. P. Lepping (1986), Major flattening of the distant geomagnetic tail, *J. Geophys. Res.*, *91*(A4), 4223–4237.
- Sibeck, D. G., R. E. Lopez, and E. C. Roelof (1991), Solar wind control of the magnetopause shape, location, and motion, *J. Geophys. Res.*, *96*(A4), 5489–5495.
- Siscoe, G. (2011), Aspects of global coherence of magnetospheric behavior, *J. Atmos. Solar-Terr. Phys.*, *73*(4), 402–419.
- Spreiter, J. R., A. L. Summers, and A. Y. Alksne (1966a), Hydromagnetic flow around the magnetosphere, *Planet. Space Sci.*, *14*(3), 223–253.
- Spreiter, J. R., A. Y. Alksne, and B. Abraham-Shrauner (1966b), Theoretical proton velocity distributions in the flow around the magnetosphere, *Planet. Space Sci.*, *14*(11), 1207–1220.
- Suvorova, A., A. Dmitriev, J.-K. Chao, M. Thomsen, and Y.-H. Yang (2005), Necessary conditions for geosynchronous magnetopause crossings, *J. Geophys. Res.*, *110*, A01206, doi:10.1029/2003JA010079.
- Taylor, M. G. G. T., et al. (2012), Spatial distribution of rolled up vortices at the dayside and flank magnetopause, *Ann. Geophys.*, *30*, 1025–1035.
- Vasyliunas, V. M. (2004), Comparative magnetospheres: Lessons for Earth, *Adv. Space Res.*, *33*(11), 2113–2120.
- Verigin, M. I., M. Tatralay, G. Erdos, and G. A. Kotova (2006), Magnetosheath-interplanetary medium reference frame: Application for a statistical study of mirror type waves in the terrestrial plasma environment, *Adv. Space Res.*, *37*(3), 715–721.
- Wang, Y. L., R. C. Elphic, B. Lavraud, M. G. G. T. Taylor, J. Birn, C. T. Russell, J. Raeder, H. Kawano, and X. X. Zhang (2006), The dependence of flux transfer events on solar wind conditions from three years of Cluster observations, *J. Geophys. Res.*, *111*(A4), A04224, doi:10.1029/2005JA011342.
- Zhang, H., M. W. Dunlop, Q.-G. Zong, T. A. Fritz, A. Balogh, and Y. Wang (2007), Geometry of the high-latitude magnetopause as observed by Cluster, *J. Geophys. Res.*, *112*, A02204, doi:10.1029/2006JA011774.
- Zhou, X.-W., and C. T. Russell (1997), The location of the high-latitude polar cusp and the shape of the surrounding magnetopause, *J. Geophys. Res.*, *102*(A1), 105–110.
- Zhuang, H. C., C. T. Russell, and R. J. Walker (1981), The influence of the interplanetary magnetic field and thermal pressure on the position and shape of the magnetopause, *J. Geophys. Res.*, *86*(1), 10009–10021.
- Zwan, B. J., and R. A. Wolf (1976), Depletion of solar wind plasma near a planetary boundary, *J. Geophys. Res.*, *81*(10), 1636–1648.